

THE VELA PULSAR AND ITS SYNCHROTRON NEBULA: AFTERMATH OF A GLITCH

D. J. HELFAND, E. V. GOTTHELF, J. P. HALPERN

Columbia Astrophysics Laboratory, Columbia University, 550 West 120th Street, New York, NY 10027, USA*Submitted to the Astrophysics Journal Letters*

ABSTRACT

We present high-resolution *Chandra* X-ray observations of PSR B0833-45, the 89 ms pulsar associated with the Vela supernova remnant. We have acquired two observations of the pulsar separated by one month to search for morphological changes in the pulsar and its environment following an extreme glitch in its rotation frequency. We find a well-resolved nebula with a morphology remarkably similar to the torus-like structure observed in the Crab Nebula, along with an axial Crab-like jet. The flux from the pulsar is found to be steady to within 0.75%; the 3σ limit on the fractional increase in the pulsar's X-ray flux is $\lesssim 10^{-5}$ of the inferred glitch energy. We use this limit to constrain parameters of glitch models and neutron star structure. We do find a significant increase in the flux of the nebula's outer torus; if associated with the glitch, the inferred propagation velocity is $\sim 0.5c$, similar to that seen in the brightening of the Crab Nebula wisps.

We propose an explanation for the X-ray structure of the Vela synchrotron nebula based on a model originally developed for the Crab Nebula. In this model, the bright, arc-shaped X-ray wisps are the shocked termination of a relativistic equatorial pulsar wind which is contained within the surrounding kidney-bean shaped synchrotron nebula which comprises the post-shock, but still relativistic, flow. In a departure from the Crab model, the magnetization parameter σ of the Vela pulsar wind is required to be of order unity; this is consistent with the simplest MHD transport of magnetic field from the pulsar to the nebula, where $B \leq 4 \times 10^{-4}$ G. The inclination axis of the equatorial torus with respect to the line of sight is identical to that of the rotation axis of the pulsar, previously measured from the polarization of the radio pulse. The projection of the rotation axis on the sky may also be close to the direction of proper motion of the pulsar if previous radio measurements were confused by orthogonal mode polarized components. We review effects that may enhance the probability of alignment between the spin axis and space velocity of a pulsar, and speculate that fast-period, slowly moving pulsars are just the ones best-suited to producing synchrotron nebulae with such aligned structures. Previous interpretations of the compact Vela Nebula as a bow-shock in a very weakly magnetized wind suffered from data of inadequate spatial resolution and less plausible physical assumptions.

Subject headings: pulsars: general — pulsars: individual (PSR B0833-45) — X-rays: general — supernova remnant — stars: neutron

1. INTRODUCTION

Within two years of the discovery of radio pulses from CP1919+21, magnetized, rotating neutron stars were firmly established as the origin of these remarkable signals. Furthermore, the steady increase in pulse frequency recorded for all sources provided an explanation for the pulsar power source: rotational kinetic energy. The detection of a rapidly slowing 33 msec pulsar in the Crab Nebula solved the long-standing mystery of what powered this unique nebula: the spin-down rate of the Crab pulsar implied an energy loss rate, $\dot{E} \sim 5 \times 10^{38}$ erg s⁻¹, more than enough to cover the radiation losses observed from radio to gamma ray frequencies. By 1974, the basic model of the electrodynamics of pulsar magnetospheres and their coupling to the surrounding synchrotron emitting plasma was in place (Rees and Gunn 1974), although a detailed understanding of the processes involved continues to elude us (e.g., Arons 1998).

A few years later, it became clear that most pulsars were not defect-free clocks which simply slowed smoothly as rotational energy was transformed into an electromagnetic outflow. Two distinct types of non-monotonic behavior were established: “timing noise” characterized by

a stochastic wandering in pulse phase and/or frequency which appeared to afflict most pulsars (Helfand, Taylor, and Backus 1980; Cordes and Helfand 1980; Cordes and Downs 1985; D'Amico et al. 1998), and “glitches”, an apparently instantaneous increase in the pulse frequency (a spin-up) accompanied by a simultaneous change in the spin-down rate; these rare events were found to be most prevalent in young objects (Reichly and Downs 1971; Lyne 1996 and references therein). Thirty years after the first glitch in the Vela pulsar was recorded, a total of 65 events have been seen from 27 different pulsars (Lyne 1996; Wang et al. 2000).

Glitches produce sudden fractional increases in the pulsar spin frequency $\delta\nu/\nu \approx 10^{-9}$ to 6×10^{-6} . No pulsar with a characteristic age of $> 10^6$ yr has been observed to glitch more than once, but some young objects experience these events roughly annually. The best studied and most prolific in terms of large glitches is the first object in which a glitch was seen – the Vela pulsar. A dozen events have been recorded over the past three decades and daily monitoring continues. Last January, the largest event yet recorded occurred: $\delta\nu/\nu = 3.14 \times 10^{-6}$.

Several models have been advanced to explain the sud-

den apparent change in the moment of inertia of a glitching neutron star. Originally, starquakes, resulting from the release of strain in the stellar crust induced by the change in the equilibrium ellipticity of the star as it slows, were invoked (Ruderman 1969). But the magnitude and frequency of the Vela glitches could not be explained by this model, and a picture involving the sudden unpinning from the inner crust of superfluid vortices in the core of the star became the dominant paradigm (Anderson and Itoh 1975). Observations of the relaxation of the star back toward its original spin-down rate suggest that $\sim 1\%$ of the star's mass is involved in the event (Alpar et al. 1988; Ruderman, Zhu, and Chen 1998), implying a total energy release of $\sim 10^{42}$ ergs.

The fate of this energy is unclear and predictions concerning the observable consequences vary widely. The timescale for energy deposited at the base of the crust to diffuse outward, the fraction of the surface area whose temperature will be affected, and the secondary effects, such as the rearrangement of the surface magnetic field which could dump energy into the surrounding synchrotron nebula, are all uncertain by one or more orders of magnitude. Because of these large theoretical uncertainties, the observation of a pulsar on a variety of timescales following a large glitch is guaranteed to eliminate large swathes of parameter space describing otherwise inaccessible quantities such as the heat capacity of neutron star material, the depth of the glitch, the diffusion properties of the crustal matter, and the coupling of the magnetosphere to the surrounding nebula.

In this paper, we report new results on PSR B0833-45 based on recent observations acquired with the *Chandra* High Resolution Camera. The data enable us for the first time to distinguish morphological details of the nebula surrounding PSR B0833-45, and reveal a striking picture of bilateral symmetry reminiscent of the loops and jets recently resolved in the Crab Nebula (Weisskopf et al. 1999). We offer an interpretation of the nebula's structure which requires an MHD wind with a high magnetization parameter (unlike that inferred for the Crab). We also construct a high quality soft X-ray pulse profile and set tight upper limits on any change in the profile following the glitch, constraining models for the neutron star interior. Finally, we demonstrate an apparent brightening in the Nebula a month after the spin-up event; whether this was stimulated by the glitch, or is a phenomena akin to the brightening wisps in the Crab Nebula remains a question for future observations to answer.

In section 2, we describe in some detail the analysis procedures required to extract quantitative information from our HRC data, in part as a cautionary tale for other early users of this instrument. We then go on to delineate the morphology of the pulsar's synchrotron nebula (§3), the soft X-ray pulse profile and limits on changes thereto (§4), and a search for changes in the nebula following the glitch (§5). The Discussion (§6) begins by developing a model which accounts for the Nebula's geometry with respect to the pulsar, as well as its anomalously low value of L_x/\dot{E} ; we then go on to derive constraints on glitch models from the temporal changes we see (and don't see) following the glitch. The final section (§7) summarizes our conclusions and assesses the prospects for future observations.

2. OBSERVATIONS

In response to an IAU Circular announcing a large Vela glitch on January 16.319 (Dodson et al. 2000), we submitted a Target of Opportunity request to the *Chandra* Observatory (Weisskopf et al. 1996) to observe the pulsar as soon as practical, followed by a second observation roughly one month later in order to search for changes in the pulsar's flux, pulse profile, and/or surrounding nebula. The observations were carried out on 20 January 2000 and 21 February 2000, ~ 3.5 and ~ 35 days after the glitch using the *Chandra* imaging High Resolution Camera (HRC-I; Murray et al. 1997). Integration times of ~ 50 ksec were achieved in both observations.

The HRC-I detector on-board *Chandra* is sensitive to X-rays over the 0.08–10.0 keV range, although essentially no energy information on the detected photons is available. Photons are time-tagged with 15.6 μ s precision; in this work, their arrival times were corrected to the solar system barycenter using a beta version of **AXBARY**. The data were collected during a portion of the orbit which avoided regions of high background contamination such as from the bright Earth and from radiation belt passages; the second observation was, however, found to be partially contaminated by particle activity likely of solar wind origin (see below). The pulsar was centered at the on-axis position of the HRC where the point-spread function (PSF) has a minimum half-power radius (the radius enclosing 50% of total source counts) of $\sim 0''.5$, which increases with energy. HRC images of the PSR B0833-45 were extracted centered on the pulsar and binned using the native HRC $0''.13175 \times 0''.13175$ pixel size into 1024×1024 pixel images (2.5' on a side).

We began our analysis using event data calibrated by the initial processing and made available through the *Chandra* public archive. The first observation revealed several problems in the standard data sets and further problems were subsequently found during the analysis of the second observation. These problems affected the spatial and timing analysis and had significant implications for the proper interpretation of the data. We alerted the HRC hardware and software teams to the instrument and data processing anomalies, and received considerable support in working through the problems. We document here the various artifacts discovered and the steps taken to correct for, or eliminate, them in our final data sets; our goals in doing so are 1) to allow others to replicate our results, and 2) to alert other early HRC users to problems they may encounter. In fact, we found it necessary to reprocess the data from Level 0.5 using custom scripts which incorporated improved filtering and processing tools, making use of several beta versions of software provided by the HRC team.

In the first observation we found evidence for a significant "ghost image" which appeared as a spectacular jet-like feature emanating from the pulsar along the detector v -axis. Examination by the instrument team found that the standard processing failed to screen out all events flagged as instrumental. After filtering with a beta version of **SCREEN_HRC** with the mask parameter set to 32771, a much truncated jet-like feature was still apparent. In order to isolate any detector-centric artifacts, we obtained the second observation with a roll angle offset by 36 de-

grees from the first. As discussed below, we were able to confirm the reality of the residual jet-like feature in the cleaned images.

Independent of any filtering, the initial images showed the pulsar to be broader than the nominal PSF. To separate the pulsar from any proximate nebular emission, we followed the same phase-resolved imaging analysis described in Gotthelf & Wang (2000) for the HRC observation of PSR 0540–69, the 50 ms pulsar in the LMC. This separation, however, failed completely. By plotting the arrival times of the pulsar centroid, we observed that the sky coordinates of the pulsar wandered in a sinusoidal fashion with an amplitude of $0.3''$ and the periodicity of the programmed telescope dither. This accounted for the pulsar's non-point-like appearance in the time-integrated image. Discussions with the *Chandra* attitude aspect team, however, showed a high-quality aspect reconstruction for the Vela observations.

Further analysis by the HRC team revealed a systematic problem with one of the three anode preamplifiers which causes the coarse position algorithm to mis-place photon locations depending on the photon input position relative to the HRC tap gaps. This explains the apparent wandering of the pulsar centroid at the dither frequency: a fraction of the detected photons are displaced along the detector coordinates by a fixed amount. Indeed, we were able to identify that the apparent diffuse flux was produced by faint echoes of the pulsar itself along the orthogonal directions of the detector axis¹.

To eliminate the echoes, we initially used the bright pulsar as a fiducial point to re-aspect the field photons and thus take out the detector-induced wobble in a statistical sense. Subsequently, the instrument team made available a beta version of a code to identify and correct the mis-placed photons – `HRC_EVT0_CORRECT` – along with updated degap parameters ($cfu1 = 1.068$; $cfu2 = 0.0$; $cfv1 = 1.045$; $cfv2 = 0.0$) for use in `HRC_PROCESS_EVENTS`. This software, together with the new parameters, effectively eliminated the echo problem. The images produced by the two methods are indistinguishable and the pulsar now matches the PSF to within its estimated uncertainty.

In the second Vela observation, we noted additional artifacts in the sky image resembling a rabbit-ear antenna, extending $20''$ from the pulsar in orthogonal directions along the detector axes, with point-like sources at the ends. Temporal analysis of the region showed that the rabbit-ear counts occurred during a number of specific time intervals lasting tens of seconds. Examination of the mission time line parameters showed that the occurrence of these events always followed the “AOFF_GAP” times by a few hundred seconds. Furthermore, data drop-outs were found for tens of seconds at the “AOFF_GAP” times and during the following intervals when the spurious counts were recorded. We wrote an algorithm to generate a new good-time-intervals file which eliminates these intervals based on the “AOFF_GAP” times.

Two additional detector issues needed consideration when extracting accurate timing information: telemetry saturation and a hardware time-stamp mis-assignment. Although data obtained during the first Vela observation was virtually free of non-X-ray background contamination,

the second observation was plagued by intervals of telemetry saturation induced by high background levels; such occurrences can seriously affect timing studies by introducing spurious periods in the power spectrum aliased with the full buffer rate of ~ 4 ms. We filtered out telemetry-saturated time intervals with the dead time fraction criteria of $DFT > 0.9$. A further complication for precision timing was recently discovered by the hardware team: the time-stamps for each event are mis-assigned to the following event. Based on the `VALID_EVT_COUNT` count rate of ~ 500 cps, the average error in the assigned photon arrival time is 2 ms or a 2% phase error for the Vela pulsar; assuming roughly Poisson fluctuations in the HRC count rate over the observation interval, the maximum error for any photon will be ≤ 3 ms. Thus, with 25 phase bins across the 88 msec pulsar period, few, if any, photons have been misassigned and we have taken no mitigating action to correct this error.

To compare directly the two Vela observations, we reprocessed both data sets starting from the Level 0.5 event files using identical methods and filter/screening/processing criteria, compensating for incorrect keyword values, producing correct GTI extensions, etc. This resulted in a total of 50.3 ks and 45.3 ks integration times for the first and second observation, respectively. Despite all the initial discrepancies and artifacts in the two observations, this reprocessing produced effectively identical images, light curves and count rates. We are thus confident that we have eliminated all currently recognized instrumental artifacts in the final Vela data sets upon which we base our analysis herein.

3. AN IMAGE OF THE VELA PULSAR

A global view of the Vela pulsar and its environment as seen by the *Chandra* HRC is presented in Figure 1. The pulsar is embedded in a complex region of previously resolved thermal X-ray emission from the Vela supernova remnant.

The superb spatial resolution of the *Chandra* HRC provides the first look at the structure of the synchrotron nebula in the immediate vicinity of PSR B0833-45; Figure 2 shows an image constructed from the two observations which have been centered on the pulsar and co-added. The bright point source representing the pulsar has an extent roughly consistent with the local PSF. Apparently emanating from the pulsar, towards the southeast, is a linear, jet-like feature $10''$ in length. There is also evidence for a counter jet in the opposite direction from the pulsar. These jets are aligned to within 13 ± 5 degrees with the pulsar's proper motion vector (DeLuca, Mignani, and Caraveo 2000).

Concentric with the pulsar is a diffuse outer arc of emission perpendicular to the jet-like feature. This feature is roughly elliptical in shape and extends over a cone angle of ~ 120 degrees. Interior to this arc is an elliptical ring of emission with a curvature very similar to the outer arc. The pulsar, jet, and arcs are embedded in a extended nebula of faint diffuse emission which is roughly “kidney-bean” shaped (Markwardt and Ogelman 1998). The configuration of the jet feature relative to the nebula

¹This problem does not effect early HRC-I observations, such as for the 50 ms pulsar PSR 0540–69 (see Gotthelf & Wang 2000), that were obtained before the gain was reduced by a factor of two.

is reminiscent of the *Chandra* image of the Crab Nebula (Fig. 3; see Weisskopf et al. 1999).

We determined the count rates by extracting counts from the various regions discussed above. For each source region we carefully estimated the background. For the diffuse emission we determined the HRC detector background derived from an annulus 13.2" wide exterior to the kidney bean emission ($r > 52.7''$). We extracted counts from the pulsar using a circular aperture 2''.64 in diameter and estimated background from the surrounding annulus, $2''.635 < r < 3''.426$. Table 1 summarizes the properties of the individual components, including their PSF-corrected sizes and intensities.

The best current measurements for the Vela pulsar and remnant place it at a distance of only 250 ± 30 pc (Cha, Sembach, and Danks 1999 and references therein); in all that follows we scale by $d = 250d_{250}$ pc.

Vela X, the $\sim 100'$ diameter, flat-spectrum radio component near the center of the Vela remnant (Milne 1968) is generally regarded as the pulsar's radio synchrotron nebula. While soft X-rays from this region are detected, they are primarily thermal in nature, and represent emission from the hot plasma which fills the entire remnant (Kahn et al. 1985). The compact X-ray source near the pulsar was first recognized by Kellogg et al. (1973) as having a harder spectrum. Subsequent observations with increasing angular resolution (Harnden et al. 1985 and references therein; Ogelman, Finley, and Zimmermann 1993; Markwardt and Ogelman 1998) localized the compact nebula to a region $\sim 2'$ in extent roughly centered on the pulsar. Ogelman et al. (1993) used the nominal PSF of the ROSAT PSPC and an *ad hoc* model for the surface brightness of the diffuse emission to attempt a deconvolution of the pulsar and its nebula and to obtain spectral fits to the two components. They found that a blackbody effective temperature of 0.15 keV adequately characterized the point source, while the extended emission exhibited a power law spectrum with a photon index of ~ 2.0 ; a column density of $N_H = 1 \times 10^{20} \text{ cm}^{-2}$ is marginally consistent with both fits. Markwardt and Ogelman (1998) subsequently revised the division of the flux between the point source and nebula based on ROSAT HRI observations. Seward et al. (2000) attempted to isolate the pulsar emission temporally and found somewhat lower blackbody temperatures. The RXTE observations of Gurkan et al. (2000) found a similar power law index for the nebula, but a much higher normalization; while this could indicate diffuse synchrotron X-ray emission from a larger area (given their one-degree field of view), it could also result from background modeling problems, since Vela is a weak source for RXTE.

As described above, our HRC image allows us to separate cleanly the pulsar from the nebular emission. We find count rates for the pulsar and the nebula minus the pulsar (within a radius of 50'') completely consistent with those of Markwardt and Ogelman (1998) using the Ogelman et al. (1993) spectral parameters ($kT = 0.15 \text{ keV}$; $N_H = 1 \times 10^{20} \text{ cm}^{-2}$), confirming these as a useful characterization of the observed flux. This leads to an unabsorbed, bolometric luminosity for the pulsar blackbody emission of $1.5 \times 10^{32} d_{250}^2 \text{ erg s}^{-1}$. Note, however, that this luminosity is inconsistent with the adopted temperature ($T = 1.7 \times 10^6 \text{ K}$) and distance (250 pc) for a uniformly radiating blackbody with a radius of 10 km; even for the minimum neutron star radius

consistent with reasonable equations of state ($R \sim 7 \text{ km}$), the derived L_x is too high by a factor of 20. Lowering T to $8.5 \times 10^5 \text{ K}$ as advocated by Seward et al. (2000) yields self-consistent values for L_x , R, T, and d, and raises the intrinsic luminosity by $\sim 30\%$. Adjusting the distance, and including such effects as radiative transport in the neutron star atmosphere and a non-uniform temperature distribution over the surface will also affect the calculated luminosity. For the purpose of a comparison with glitch models (§6), we adopt $T = 1.0 \times 10^6 \text{ K}$.

The integrated luminosity of the nebula in the $0.1 - 10$ keV band is $3.5 \times 10^{32} d_{250}^2 \text{ erg s}^{-1}$, corresponding to 4.9×10^{-5} of the pulsar's spin down luminosity. This ratio of L_{neb}/\dot{E} is significantly lower than that for any other pulsar, and is a major constraint on models for coupling the pulsar wind to the nebula (see §6).

4. THE X-RAY PULSE PROFILE

After many unsuccessful searches, Ogelman et al. (1993) were the first to detect X-ray pulsations from the Vela pulsar using the ROSAT PSPC. Their observations revealed a complex profile, not obviously related to the pulse profiles previously recorded at radio, optical, and gamma-ray wavelengths. The observed pulsed fraction of $4.4 \pm 1.1\%$ was diluted by the inability of the PSPC to resolve the pulsar from the surrounding nebula; using the approximate model described above, the authors estimated a soft X-ray pulsed fraction of 11%. Seward et al. (2000) constructed a higher signal-to-noise profile by combining six ROSAT HRC observations; they estimated a pulsed fraction of 12% divided between a broad component (8%) and two narrow peaks (4%). Strickman et al. (1999) and Gurkan et al. (2000) have recently shown 2-30 keV profiles based on RXTE observations of Vela. The former authors illustrate a trend in which the component separation of the main pulse increases with energy.

We have determined the X-ray pulse period for our two observations and compared them to the radio ephemeris. We began by constructing a periodogram around a narrow range of periods centered on the expected period $\pm 0.1 \text{ ms}$, sampled in increments of $0.05 \times P^2/T$, where T is the observation duration, and P is the test period. For each trial period, we folded photons extracted from a 2''.64 diameter aperture centered on the pulsar position using 25 phase bins and computed the χ^2 of the resultant profile. We find a highly significant signal ($> 8\sigma$) at $P = 89.32842(5) \text{ ms}$ at epoch 51563.314043 MJD and $P = 89.32876(6) \text{ ms}$ at epoch 51595.370251 MJD; the uncertainty is estimated according to the method of Leahy (1987). We have assumed a period derivative of $\dot{P} = 1.258 \times 10^{-13}$ for the interval encompassing the two observations. Our results are consistent (within the errors) with the radio-derived ephemeris.

The relative phase offset between the start times of our two observations is computed empirically by cross correlating the two profiles; we offset the second profile by 0.64 in phase and coddled the two datasets. The $\sim 200,000$ counts, uncontaminated by nebular emission, provides us with the highest signal-to-noise X-ray pulse profile for Vela yet reported (Figure 4). Greater than 99% of the counts from the blackbody component detected by the HRC fall in the $0.1 - 2.4 \text{ keV}$ ROSAT band, and we confirm a pulsed

TABLE 1
HRC SPATIAL COMPONENTS OF PSR B0833-45

Component ^a	PSR B033-45 System Shape and Size	Counts s ⁻¹ ^b	Crab System Shape and Size
Pulsar (Obs 1)	point-like	2.012 ± 0.006	point-like
(Obs 2)		1.997 ± 0.007	
Nebula (Obs 1)	20'' × 10'' NE-SW	2.720 ± 0.007	2' × 10' NE-SW
(Obs 2)		2.762 ± 0.008	
Jet (Obs 1)	10'' long SE-NW	0.037 ± 0.001	45'' long SE-NW
(Obs 2)		0.036 ± 0.001	

^aSee §3.

^bCount rates are background subtracted.

fraction of 12%. We measure a separation between the two peaks of the main component of $\delta\phi \sim 0.325$, consistent with a linear extrapolation of the energy-dependence of this quantity reported by Strickman et al. (1999).

The background-corrected pulsar count rates were found to be 2.012 ± 0.006 and 1.997 ± 0.007 cps, respectively, for the first and second epochs; the overall count-rate is constant to within 0.75% (the second observation is 1.5σ fainter than the first). Thus, the 3σ limit on any increase in the pulsar luminosity in response to energy input from the glitch is $< 1.2 \times 10^{30}$ erg s⁻¹ or $\Delta T \sim 0.2\%$, 35 days (3×10^6 s) after the event². The lower half of Figure 4 shows the difference as a function of pulse phase between the two observations, where the second dataset has simply been scaled by the ratio of the total integration times; no single bin has a discrepancy exceeding 1.5 sigma. This constancy in both the pulsed luminosity and pulse profile set interesting constraints on the glitch mechanism (see §6).

5. CHANGES IN THE NEBULA

While the primary energy release from a glitch must be within (or on the surface of) the neutron star, the response of the star's magnetosphere could result in the release of energy to the synchrotron nebula, triggering changes in its morphology and/or brightness. Even without the stimulus of a glitch, the optical wisps of the Crab Nebula near the pulsar have been shown to change on timescales of weeks in response to instabilities in the relativistic wind from the pulsar (Hester et al. 1995). Thus, we have examined our two images of the Vela Nebula carefully in a search for surface brightness fluctuations.

We examined the count rate in the kidney bean region bracketed by the outer-arc and an inner circle with $r = 1''.32$ centered on the pulsar. No significant change was observed between the two observations. Similarly no measurable change in the count rate associated with the jet-like feature was found. Comparisons of other regions defined in Table 1 also showed no change, with the notable exception of the outer arc itself which appeared to increase

in brightness in the second observation by $\sim 5\%$.

To investigate this further, we examined regions congruent with the morphology of the nebula by constructing radial bins which are elliptical in shape; the ratio of semi-major to semi-minor axes of the ellipse, $a/b = 1.76$, and the elliptical annuli are oriented at a position angle of 50 degrees (east of north). As Figure 5 shows, the sector of the radial profile encompassing the bright northwest arc (see range below) exhibits a 7.8σ excess between semi-minor axis radii of $13.5''$ and $18.0''$ in the sense that the source is brighter in the second observation. No other sectors or radii show any significant changes. In Figure 6, we display an azimuthal profile of the whole nebula in the elliptical ring $4.5''$ wide centered on these radii, measured clockwise from the jet; North lies at 130° . The residuals are positive (the second observation is brighter) throughout the range 110° to 260° ; the excess is significant at the 7.6σ level and represents a brightening of 5.3%. The excess energy being radiated in the HRC band amounts to $\sim 3 \times 10^{30}$ erg s⁻¹. For a distance of 250 pc, the outer arc lies at a projected distance of 3×10^{16} cm from the pulsar, requiring signal propagation at $\sim 0.5c$, assuming the impetus for the brightening originated from the pulsar at the time of the glitch.

6. DISCUSSION

6.1. Geometry and Kinematics of the Nebular Structure

Figures 6 and 7 show our proposed model for an equatorial wind interpretation of the X-ray wisps in the Vela pulsar. We first describe the geometry and inferred kinematics of this structure. The details of the physical model will be presented in §6.3. We assume that the two prominent arc-like features lie along circular rings highlighting shocks in which the energy of an outflowing equatorial wind is dissipated to become the source of synchrotron emission for the compact plerion extending to the boundary of the “bean”. One reason that the wisps are not complete rings might be that the emission is from outflowing particles which Doppler boost their emission in the forward direction.

²This estimate includes a $\sim 20\%$ correction for the fraction of the bolometric luminosity lying outside the HRC band.

This is essentially the Arons (1998) picture of the similar wisps surrounding the Crab pulsar, except that the dark cavity which contains the unshocked pulsar wind in the Kennel & Coroniti (1984a) model of the Crab is small compared with the volume of the Crab nebula, while the radius of the Vela plerion (the bean), is not even twice as large as its pulsar wind cavity. We assume that the two rings straddle the equator symmetrically, and suppose that the deficit of emission exactly in the equatorial plane is related to the fact that this is where the direction of a toroidally wrapped magnetic field changes sign; i.e., the field may vanish there. The semimajor axis of the ring $a = 35''$, and the ratio $a/b = 1.76$ specifies the angle that the axis of the torus (i.e., the rotation axis of the pulsar) makes with the line of sight, $\zeta = \cos^{-1}(b/a) = 55.4^\circ$. The angle $\Psi_0 = 130^\circ$ is the position angle of the axis of the torus on the plane of the sky, defined according to convention as the angle measured to the east from north. The direction of rotation (sign of Ω) is arbitrary.

The projected separation of the two rings is measured as $s = 13''$. The half opening angle of the wind θ is then given by $\tan \theta = s/(2a \sin \zeta) = 0.225(\theta = 12.7^\circ)$, and the radius of the shock is $r_s = a d / \cos \theta$, where d is the distance to the pulsar. For $d = 250$ pc we find $r_s = 1.34 \times 10^{17}$ cm.

The rotating vector model of pulsar polarization (Radhakrishnan & Cooke 1969) is commonly used to derive information about the geometry of the pulsar magnetic inclination and viewing angles. The angles ζ and Ψ_0 can in principle be evaluated independently using information derived from polarization measurements of the radio pulse. In particular, the swing in position angle $\Psi(t)$ of linear polarization across the pulse is very sensitive to ζ , the angle between the line of sight and the rotation axis. The angle α between the magnetic axis and the rotation axis is much more difficult to measure unless $\alpha \approx \zeta$ – i.e., unless the line of sight passes near the center of the polar cap. Accordingly, α is often assumed while ζ is fitted. For example, Krishnamohan & Downs (1983) assume $\alpha = 60^\circ$ in their model for Vela. When an interpulse is observed, α is often inferred to be 90° (that is, both polar caps are visible in this case). With these definitions (See Figure (8) or Figure (13) of Krishnamohan & Downs (1983) for the geometry),

$$\tan(\Psi(t) - \Psi_0) = \frac{\sin \phi(t)}{\cot \alpha \sin \zeta - \cos \zeta \cos \phi(t)}. \quad (1)$$

Here $\phi(t)$ is the longitude of the emitting region, which increases linearly with time, and Ψ_0 is the position angle of the rotation axis of the pulsar projected on the sky as in Figure (7).

In the context of the rotating vector model, Ψ_0 is identical to the position angle of polarization Ψ at the peak of the pulse where the magnetic dipole axis crosses the rotation axis ($\phi(t) = 0$ in Equation (1)). Because the emission mechanism is thought to be curvature radiation from particles moving along magnetic field lines, the electric vector is tangent to those field lines, rather than perpendicular to them as is the case with synchrotron radiation. While this measurement is in principle straightforward, in practice it is not routinely accomplished. Observations at two or more frequencies are needed to determine (and to correct

for) the interstellar rotation measure, and to demonstrate that the intrinsic polarization is in fact frequency independent. Another complication is that a pulse is often composed of several identifiable components, some of which can be polarized in the orthogonal mode (a result of propagation effects in the magnetosphere) obscuring the “true” polarization. Furthermore, the pulse itself might not even contain an identifiable core component, being composed instead of emission from random patches within a cone (e.g., Deshpande and Rankin 1999). Accordingly, measurements of Ψ_0 are rarely attempted, measurements of α are rarely trusted, and measurements of ζ are rarely questioned.

In fact, there are several determinations of Ψ_0 for the Vela pulsar that are not in particularly good agreement with each other; we review a representative subset here. The original value of Radhakrishnan & Cooke (1969) is $\Psi_0 = 47^\circ$ with an uncertainty of $\approx 5^\circ$. Hamilton et al. (1977) made measurements over several years, all of which are consistent with $\Psi_0 = 64^\circ \pm 1.5^\circ$. A detailed decomposition into four separate pulse components was performed by Krishnamohan & Downs (1983), in which they concluded that one of the components was polarized in the mode orthogonal to the other three. However, they did not attempt an absolute measurement of the angle Ψ_0 . Bietenholz, Frail, & Hankins (1991) measured $\Psi_0 = 35^\circ$ using the VLA. Thus, while the published values of Ψ_0 differ by as much as 30° , it appears that none is even close to being aligned with the axis of the nebula, and that all are roughly perpendicular to it.

Interestingly, the model of Krishnamohan & Downs (1983) produces an extremely accurate value of the angle between the rotation axis and the line of sight, $\zeta = 55.57 \pm 0.15^\circ$, and this value agrees exactly with the inclination angle of our postulated equatorial wind torus to the line of sight. By fitting an ellipse to the shape of the X-ray features we found $\zeta = \cos^{-1}(b/a) = 55.4^\circ$. This striking coincidence gives us courage to pursue the basic physics of the equatorial wind model using the geometry of Figures 7 and 8, and even to be so bold as to suggest that *all* of the radio determinations of Ψ_0 for Vela are incorrect by 90° because of incorrect mode identification (i.e., perhaps three out of four of the pulse components are actually polarized in the orthogonal mode). In this case, $\Phi_0 = 130^\circ$ (as inferred from the orientation of the X-ray torus), and can be identified with the projected direction of the pulsar rotation axis. Speculations about the true orientation of Φ_0 in pulsars go back to Tademaru (1977), who first discussed the possible alignment between spin axis and proper motion in the context of the radiation rocket hypothesis (Harrison & Tademaru 1975).

6.2. Implications of the Proper Motion

For both the Crab and Vela pulsars, the direction of proper motion (transverse velocity v_t) is strikingly close to the projected X-ray symmetry axis of the inferred equatorial wind and polar jet structures. The proper motion of the Vela pulsar was measured from *HST* images by De Luca et al. (2000). The resulting $0.052 \pm 0.003 \text{ yr}^{-1}$ at a position angle of $297^\circ \pm 2^\circ$ is within 13° of the axis of the nebula ($\phi_0 + 180^\circ = 310^\circ$). The transverse velocity $v_t = 65 \text{ km s}^{-1}$ at $d = 250$ pc. The proper motion of the Crab pulsar is $0.018 \pm 0.003 \text{ yr}^{-1}$ at a position angle of

$292^\circ \pm 10^\circ$ (Caraveo & Mignani 1999), which corresponds to $v_t = 123 \text{ km s}^{-1}$ at $d = 2000 \text{ pc}$. The axis of the Crab's toroidal optical and X-ray structure is 299° (Hester et al. 1995), only 7° from the direction of proper motion. The probability that two such close alignments will occur by chance when drawn from a pair of uncorrelated distributions is 1.1%. We also note that both Vela and the Crab are rather slow movers with respect to the typical pulsar; Lyne & Lorimer (1994) found a mean velocity for young pulsars between 400 and 500 km s^{-1} .

If these relationships are not a coincidence, then they may be understandable in terms of the scenario proposed by Spruit & Phinney (1998) who suggested that the rotation axes and space velocities of pulsars could be connected through the nature of the "kicks" given to neutron stars at birth. Spruit & Phinney argue that the rotation rate of the progenitor stellar core is too slow in the few years before the formation of the neutron star for pulsar spin periods to be explained by simple conservation of angular momentum during core collapse. Instead, it is likely that the same asymmetric kicks (whatever the cause) that are responsible for the space velocities of pulsars, are also the dominant contributors to their initial spin rates. If neutron stars acquire their velocity from a single momentum impulse, then their rotation axes should be perpendicular to their space velocities. If, however, they receive many random, independently located impulses over time, as might result from convection which leads to anisotropic neutrino transport or from anisotropic fallback, then their velocities and spins should be uncorrelated in direction. However, if those multiple thrusts are not short in duration relative to the resulting rotation period, it is possible that kicks applied perpendicular to the rotation axis will average out, while those that are along the rotation axis will accumulate. In the latter case, particularly germane for short rotation periods, the space velocity will be preferentially aligned with the rotation axis. This is actually the scenario preferred by Spruit & Phinney, for which they appeal to long duration (several-second) thrusts that could result from the effect of parity violation in neutrino scattering in a magnetic field.

Thus, we speculate that the Crab and Vela pulsars have relatively low space velocities because the components of their kicks perpendicular to their rotation axes were averaged out and, as a result, their final space velocities were aligned closely with their spin axes. Since pulsars that rotate most rapidly at birth are also the ones most capable of powering synchrotron nebulae, this might argue for a stronger than average correlation of the axes of such nebulae with the proper motion directions of their parent pulsars.

Before the equatorial wisps in the Vela nebula were resolved by *Chandra*, Markwardt & Ögleman (1998) interpreted the overall shape of the nebula as seen by the *ROSAT* HRI as being determined by the space velocity of the pulsar. In particular, they noted that the outline of the nebula, which is dominated by the bean shape, resembles a bow shock whose symmetry axis at position angle 295° is identical to the direction of proper motion (297°). However, the rather uniform and gently curved outline of this structure could only be reconciled with the sharper, asymmetric curve expected of a bow shock if the space

velocity were nearly along the line of sight. Furthermore, the large absolute velocity needed for the pulsar to exceed the speed of sound in the surrounding supernova remnant forced Markwardt & Ögleman to conclude that the velocity vector is less than 22° from the line of sight. This notion of the compact Vela nebula as a bow shock also led Chevalier (2000) to a considerably different model of its physics. As we shall argue below, the *Chandra* observations do not support such a bow-shock interpretation, but instead favor a physical model in which the entire structure is a synchrotron nebula similar in physics to the Crab, but with an interesting difference in one of its parameters.

6.3. A Physical Model of the Nebula

In the basic Kennel & Coroniti (1984a,b) model of the Crab Nebula, a relativistic pulsar wind terminates in an MHD shock, which produces the nonthermal distribution of particles and post-shock magnetic field that comprise the synchrotron nebula. Although the pulsar wind is assumed to carry the entire spin-down luminosity of the pulsar, specific wind parameters such as the particle velocity and the fraction of the power carried in magnetic fields are not known *a priori*. Rather, they are inferred by using the results of the shock jump conditions to model the spectrum of the Crab Nebula, and also to match the observed radii of the MHD shock and the outer boundary of the Nebula. It is necessary to adopt outer boundary conditions; a natural one is to require the final velocity of the flow to match the observed expansion velocity of the Nebula, although it is not clear how that outer boundary condition is communicated to the inner MHD shock which is a factor of 20 smaller in radius than the outer boundary of the Crab Nebula.

A peculiar result of the Kennel & Coroniti model is that the wind magnetization parameter σ is required to be ≈ 0.003 in the Crab. That is, the fraction of power carried in B field is much less than 1%. Such a small fraction is required in order that sufficient compression occurs in the shock to convert the bulk flow energy into random energy of the particles so that they can radiate the observed synchrotron luminosity. Highly magnetized shocks would produce less radiation because there is little energy dissipation. Furthermore, highly magnetized shocks are weak because all of the energy dissipation allowed by the jump conditions is used in making the small increase in B field needed to conserve magnetic flux. The post-shock flow velocity is still relativistic.

The reason that such a small magnetization inferred for the Crab is difficult to understand is that the pulsar magnetic field energy carried out to the radius of the shock in the simplest MHD wind should be of the same order of magnitude as the spin-down power, as the following argument shows. The wind energy flux at the shock is

$$\frac{I \Omega \dot{\Omega}}{4\pi r_s^2} = \left(\frac{B_p^2 R^6 \Omega^4}{6 c^3} \right) \frac{1}{4\pi r_s^2} = \frac{B_p^2 R^6 \Omega^4}{24\pi c^3 r_s^2} \quad (2)$$

while the transported pulsar magnetic field B_s at the location of the shock is

$$B_s \approx B_p \left(\frac{R}{r_{lc}} \right)^3 \left(\frac{r_{lc}}{r_s} \right) = B_p \frac{R^3 \Omega^2}{c^2 r_s} \quad (3)$$

where r_{lc} is the radius of the light cylinder defined as $r_{lc} = c/\Omega$ and R is the neutron star radius at which the magnetic field strength is B_p . Therefore, the magnetic energy flux at r_s is

$$c \frac{B_s^2}{8\pi} \simeq \frac{B_p^2 R^6 \Omega^4}{8\pi c^3 r_s^2}, \quad (4)$$

or 3 times the value in Equation (2). While various solutions to this paradox for the Crab have been proposed, the dimensions and luminosity of the Vela synchrotron nebula are in much better accord with $\sigma \sim 1$, and therefore *Vela is a more natural realization of the Kennel & Coroniti model than is the Crab, for which the model was created.*

A basic application of the pulsar wind model to the Vela synchrotron nebula was made by de Jager, Harding, & Strickman (1996) in conjunction with their detection of Vela with the Oriented Scintillation Spectrometer Experiment (OSSE) on the *Compton Gamma-Ray Observatory*. We summarize their conclusions here. de Jager et al. noted that the unpulsed part of the hard X-ray spectrum extends with power-law photon index $\Gamma = 1.73$ up to 0.4 MeV, which implies that the synchrotron nebula radiates $\sim 2 \times 10^{33} (E_{\max}/0.4 \text{ MeV})^{0.27}$ ergs s^{-1} , or only $\sim 3 \times 10^{-3}$ of the pulsar spin-down power. The absence of an observed spectral break limits the residence time τ_r of the electrons in the nebula that radiate in this energy range to less than their synchrotron lifetime, which is $\tau_s = 5.1 \times 10^8 / (\gamma B^2)$ s. Since the electrons which radiate at the highest observed energy E_{\max} have $\gamma = [2\pi m c E_{\max} / (h e B)]^{1/2}$, the upper limit on the nebular magnetic field is $B < 20 \tau_r^{-2/3}$ G. To make use of this limit, de Jager et al. assumed that the residence time would be $\tau_r \approx r/c_s$ where $r \sim 2 \times 10^{17}$ cm, and $c_s = c/\sqrt{3}$, the velocity of sound in a relativistic plasma. For these values, $B < 4 \times 10^{-4}$ G obtains. This requirement is compatible with a strongly magnetized pulsar wind for which little change in B occurs across the shock, while the post-shock field continues to decline as $1/r$. Indeed, equation (3) predicts a pre-shock field of 2.8×10^{-4} G, and therefore the wind may remain relativistic across the nebula, which extends less than a factor of 2 in radius beyond the shock.

Such a synchrotron nebula is in approximate pressure balance with the surrounding supernova remnant. Markwardt & Ögleman (1997) found by fitting a two-temperature thermal model to the *ASCA* spectrum of the inner remnant that the thermal pressure is $\approx 8.5 \times 10^{-10}$ erg cm^{-3} . This compares well with the pulsar wind pressure at r_s , $\dot{E}/(4\pi r_s^2 c) = 1.0 \times 10^{-9}$ erg cm^{-3} . Thus, the entire compact X-ray nebula is consistent with being powered by a strongly magnetized pulsar wind shock whose still relativistic downstream flow is confined by the Vela SNR. While this appears to be a quite satisfactory model, certain details are subject to additional constraints. First, since the radiation from the nebula is so inefficient, energetic electrons must be able to escape to much larger distance scales before losing all of their energy to synchrotron radiation. Indeed, the radio luminosity of the Vela X region, $\sim 8 \times 10^{32}$ erg s^{-1} , could be one manifestation of the escaping electrons. Second, there is a natural upper energy to the synchrotron spectrum when the electron gyroradius

r_g exceeds the radius of the nebula. Since

$$r_g = 1.6 \times 10^{17} \left(\frac{B}{10^{-4} \text{ G}} \right)^{-3/2} \left(\frac{E}{100 \text{ MeV}} \right)^{1/2} \text{ cm} \quad (5)$$

this is not a restrictive limit. Thus, we find the de Jager et al (1996) description of the Vela synchrotron nebula basically in accord with the *Chandra* observations.

An alternative picture was proposed by Chevalier (2000) based on the bow-shock interpretation of Markwardt & Ögleman (1998), and a simplified version of the Kennel & Coroniti model. If the Vela synchrotron nebula is energized by a shock between a relativistic pulsar wind and the surrounding supernova remnant, then the bow shock travels at the velocity of the pulsar v_p , which necessarily exceeds the sound speed in the hot confining medium. In the first place, such a large pulsar velocity is hardly likely, since the thermal sound speed $\sqrt{dP/d\rho} \approx 875 \text{ km s}^{-1}$ in the Vela SNR according to the *ASCA* spectral analysis of Markwardt & Ögleman (1997). Markwardt & Ögleman (1998) assumed that $v_p \geq 260 \text{ km s}^{-1}$ is sufficient.

An additional consequence of this scenario, however, is that the residence time of the emitting particles in nebula is much longer than in the de Jager et al. model, $\tau_r \sim r_s/v_p$ instead of $\tau_r \sim \sqrt{3}r_s/c$. Consequently, Chevalier (2000) was forced to assume $\tau_r \sim 10^3 \text{ yr}$, requiring an extremely small magnetization parameter, $\sigma < 10^{-4}$, in order for the model's radiated luminosity not to exceed the observed X-ray luminosity. In fact, even this is insufficient if the newly determined distance of 250 pc is adopted. Using this value and the observed quantities \dot{E} , v_p , and the shock radius r_s along with the nominal values for other quantities in his equation 12, we find a predicted value for $L_x = 7.6 \times 10^{34} \text{ erg s}^{-1}$, a factor of 200 greater than that observed. We have explored the sensitivity of the predicted luminosity to the assumed particle spectral index over the range $2.05 < p < 2.5$ and find only a factor of ~ 2 range in predicted L_x . We have also varied the other parameters and find difficulty in reproducing the observed luminosity for any reasonable combination. Increasing the distance by its 3σ uncertainty to 340 pc and simultaneously decreasing the assumed moment of inertia of the neutron star by a factor of 3 (about the lowest value consistent with measured masses and acceptable equations of state) still leaves the predicted luminosity high by a factor of > 4 .

We consider that the physical difficulties of the bow-shock interpretation, in conjunction with the new *Chandra* evidence that the X-ray morphology is dominated by a pair of wisps which strongly resemble similar toroidal structures in the Crab Nebula, strongly disfavor such a model. Instead, the Vela synchrotron nebula may be a more natural fit to the well honed theories for the Crab Nebula than is the Crab itself, in that it is compatible with the simplest possible pulsar-powered MHD wind.

6.4. Thermal Emission Constraints on the Neutron Star Interior

Our stringent upper limit on a change in the X-ray flux from the neutron star within the 35 days following the glitch allow us to begin setting meaningful constraints on the parameters of the neutron star and the glitch. Seward et al. (2000) provide a concise introduction to the

published models for the thermal response of the stellar surface to a glitch generated by the sudden unpinning of superfluid vortex lines deep in the star (Van Riper et al. 1991; Chong and Cheng 1994; Hirano et al. 1997, and Cheng, Li, and Suen 1998), and we need not repeat it here. We follow their approach in deriving parameter limits from the models.

The allowable range in the pulsar's flux derived in §4 corresponds to a fractional change in the surface temperature of $< 0.2\%$. For timescales of ~ 30 days, we are primarily sensitive to stars with small radii ($R < 14$ km) which correspond to soft or moderate equations of state. Using Figure 2 of Van Riper et al. (1991), we can set a limit of $E_{\text{glitch}} < 10^{42}$ ergs independent of the depth of occurrence within the inner crust. For depths corresponding to local densities $\rho > 10^{13}$ gm cm $^{-3}$, $E_{\text{glitch}} < 3 \times 10^{41}$ ergs, and for shallow events ($\rho \sim 10^{12}$ gm cm $^{-3}$), the glitch energy must be less than 10^{41} ergs. For the softest equation of state used by Hirano et al. (1997) corresponding to a $1.4M_{\odot}$ star with a radius of 11 km, glitch depths shallower than 10^{13} gm cm $^{-3}$ require an energy deposition of less than 10^{41} ergs. With observations of similar sensitivity ~ 300 and ~ 3000 days after the event, we could rule out $E_{\text{glitch}} \sim 10^{43}$ erg for all equations of state and glitch depth combinations, and require $E_{\text{glitch}} < 10^{41}$ ergs for soft and moderate equations of state for depths $\rho < 10^{13.5}$ gm cm $^{-3}$. Note that on the longest timescales (appropriate for deep glitches in stars with very stiff equations of state), Vela may be an inappropriate target for constraining glitch parameters, since another glitch may well have occurred before the thermal pulse has peaked; indeed, if even 10% of the glitch energy appears as surface thermal emission, the total X-ray luminosity can be powered by events with $\langle E_{\text{glitch}} \rangle \sim 2 \times 10^{41}$ ergs.

7. SUMMARY AND CONCLUSIONS

We have presented a high-resolution X-ray image of the Vela pulsar revealing a highly structured surrounding nebula. We interpret the nebula's morphology in the context of the shocked MHD wind model developed by Kennel and Coroniti (1984a,b) for the Crab Nebula, and find that the Vela Nebula is a more natural realization of that model in that it requires a wind magnetization parameter of order unity. This picture also provides a natural explanation for the low L_x/\dot{E} of the Vela Nebula. We speculate that

the alignments of the symmetry axes of the Crab and Vela Nebulae with the proper motion vectors of their respective pulsars should be expected preferentially in rapidly spinning young pulsars with surrounding X-ray synchrotron nebulae if the causal connection of spin and proper motion suggested by Spruit and Phinney (1998) is correct.

Our two observations, centered 3.5 and 35 days after the largest glitch yet recorded from the pulsar, allow us to set significant limits on changes in the pulse profile and stellar luminosity which can be used to constrain glitch model parameters. We find that, for soft and moderate equations of state, the glitch energy must be $< 10^{42}$ ergs; an additional observation a year following the event will substantially tighten this constraint. An apparent change in the nebula surface brightness between the two observations may or may not be a consequence of the glitch; the implied velocity of the disturbance, assuming that it originates near the pulsar, is $\sim 0.5c$, similar to the velocity inferred from changes in the Crab Nebula wisps.

Future observations with *Chandra* and XMM can be used to gain further insight into the structure of the neutron star and its surrounding nebula. A data point ~ 350 days after the glitch will further constrain models for the glitch and the parameters of the neutron star. Additional HRC observations will also be required to decide whether the nebula changes reported here are a consequence of the glitch, or whether they occur routinely in response to instabilities in the pulsar's relativistic wind, as appears to be the case in the Crab Nebula. Data from the EPIC PN camera on XMM will yield spectral clues to help in understanding the complex pulse profile, while either EPIC or *Chandra*'s ACIS could be used to search for spectral changes caused by synchrotron energy losses and/or internal shocks in the nebula.

We are grateful to the *Chandra* Science Center Director, Dr. Harvey Tananbaum, for making this TOO possible. We also wish to acknowledge Dr. Steven Murray and Dr. Michael Juda for many extremely helpful discussions concerning HRC issues, and for kindly making available beta-version software. This work was funded in part by NASA LTSA grant NAG5-7935 (E.V.G.), SOA *Chandra* grant DD0-1002X (D.J.H), and NAG5-6035 (J.P.H.). This is contribution #692 of the Columbia Astrophysics Laboratory.

REFERENCES

Alpar, A., Cheng, K.S., Pines, D. and Shaham, J. 1988, MNRAS 233, 25

Arons, J. 1998, Mem. Soc. Astr. Ital., 69, 989

Anderson, P.W. and Itoh, N. 1975, Nature 256, 25

Caraveo, P., Mignani, R., & Bignami, G. B. 1998, in Memorie della Societa Astronomia Italiana, Vol. 69, p.1061

Caraveo, P. A., Mignani, R. P. 1999, A&A, 344, 367

Cha, A.N., Sembach, K.R., and Danks, A.C. 1999, ApJ 515, L25

Cheng, K.S., Li, Y., and Sven, W.M. 1998, Ap., 499, L45

Chevalier, R. A. 2000, ApJ Letters, submitted

Cordes, J.M. and Helfand, D.J. 1980, ApJ 239, 640

Cordes, J.M., and Downs, G.S. 1985, ApJS, 59, 343

D'Amico, N., Stappers, B.W., Bailes, M., Martin, C.F., Bell, J.F., Lyne, A.G., and Manchester, R.N. 1998, MNRAS, 297, 28

de Jager, O. C., Harding, A. K., & Strickman, M. S. 1996, ApJ, 460, 729

Deeter, J. E., Nagase, F., Boynton, P. E. 1999, ApJ, 512, 300??

DeLuca, A., Mignani, A.P., and Caraveo, P.A. 2000, A&Ap, 354, 1011

Deshpande, A.A. and Rankin, J.M. 1999, ApJ 524, 1008

Dodson, R.G., McCulloch, P.M., and Costa, M.E. 2000, IAUC 7347

Gotthelf, E. V. & Wang, Q. D. 2000, ApJ, 532, L117

Gurkan, M.A., Baykal, A., Alpar, M.A., Ögelman, H.B., and Strohmayer, T. 2000, astro-ph/0002487

Hamilton, P. A., McCulloch, P. M., Manchester, R. N., Ables, J. G., & Komesaroff, M. M. 1977, Nature, 265, 224

Harnden, F.R., Grant, P.D., Seward, F.D., and Kahn, S.M. 1985, ApJ 299, 828

Harrison, E. R., & Tademaru, E. 1975, ApJ, 201, 447

Helfand, D.J., Taylor, J.H., and Backus, P.R. 1980, ApJ 237, 206

Hester, J. J., et al. 1995, ApJ, 448, 240

Hester, J. 1998 in "The Relationship Between Neutron Stars and Supernova Remnants," ed. R. Bandiera, E. Masini, F. Pacini, M. Salvati, and L. Woltjer, Memorie della Societa Astronomica Italiana, Vol. 69, No. 4, p. 883

Kahn, S.M., Goenstein, P., Harnden, F.R., and Seward, F.D. 1985, ApJ, 299, 821

Kellogg, E., Tananbaum, H., Harnden, F.R., Gursky, H., Giacconi, R., and Grindlay, J. 1973, ApJ 183, 935

Kennel, C. F., & Coroniti, F. V. 1984a, ApJ, 283, 710

_____. 1984b, ApJ, 283, 731
 Krishnamohan, S., & Downs, G. S. 1983, ApJ, 265, 372
 Leahy, D. A., 1987, A&A, 180, 275
 Lyne, A. G., & Lorimer, D. R. 1994, Nature, 369, 127
 Lyne, A.G. 1996 in "Pulsars: Problems and Progress" ed. S. Johnston, M.A. Walker, and M. Bailes (ASP Conf. Ser. 105), p.73
 Ögelman, H.B., Finley, J.P., and Zimmermann, H.U. 1993, Nature 361, 136
 Markwardt, C. B., & Ögelman, H. B. 1997, ApJ, 480, L13
 Markwardt, C. B., & Ögelman, H. B. 1998, Mem. Soc. Astr. Ital., 69, 927
 Milne, D.K. 1968, Aust.J.Phys. 21, 206
 Murray, S. S., et al., 1997, SPIE, 3114, 11
 Radhakrishnan, V., & Cooke, D. J. 1969, Ap Lett, 3, 225
 Rees, M.J. and Gunn, J.E. 1974, MNRAS 167, 1
 Reichley, P.E. and Downs, G.S. 1971, Nature Phys. Sci. 234, 48
 Ruderman, M.A. 1969, Nature 223, 597
 Ruderman, M.A., Zhu, T. and Chen, K. 1998, ApJ 492, 267
 Seward, F.D., Alpar, M.A., Flanagan, C., Kiziloglu, U., Markwardt, C., McCulloch, P., Ögelman, H. 2000, astro-ph/0004015
 Spruit, H., & Phinney, E. S. 1998, Nature, 393, 139
 Strickman, M.S., Harding, A.K., and de Jager, O.C. 1999, ApJ 524, 373
 Tademaru, E. 1977, ApJ, 214, 885
 Wang, Q. D. & Gotthelf, E. V. 1999, ApJ, 509, 109
 Wang, N., Manchester, R.N., Pace, R.T., Bailes, M., Kaspi, V., Stappers, B.W., & Lyne, A.G. 2000, MNRAS (in press)
 Weisskopf, M. C. O'Dell, S. L., van Speybroeck, L. P. 1996, Proc. SPIE 2805, Multilayer and Gazing Incidence X-ray/EUV Optics III, 2.
 Weisskopf, M.C. et al. 1999, BAAS 31, 1540

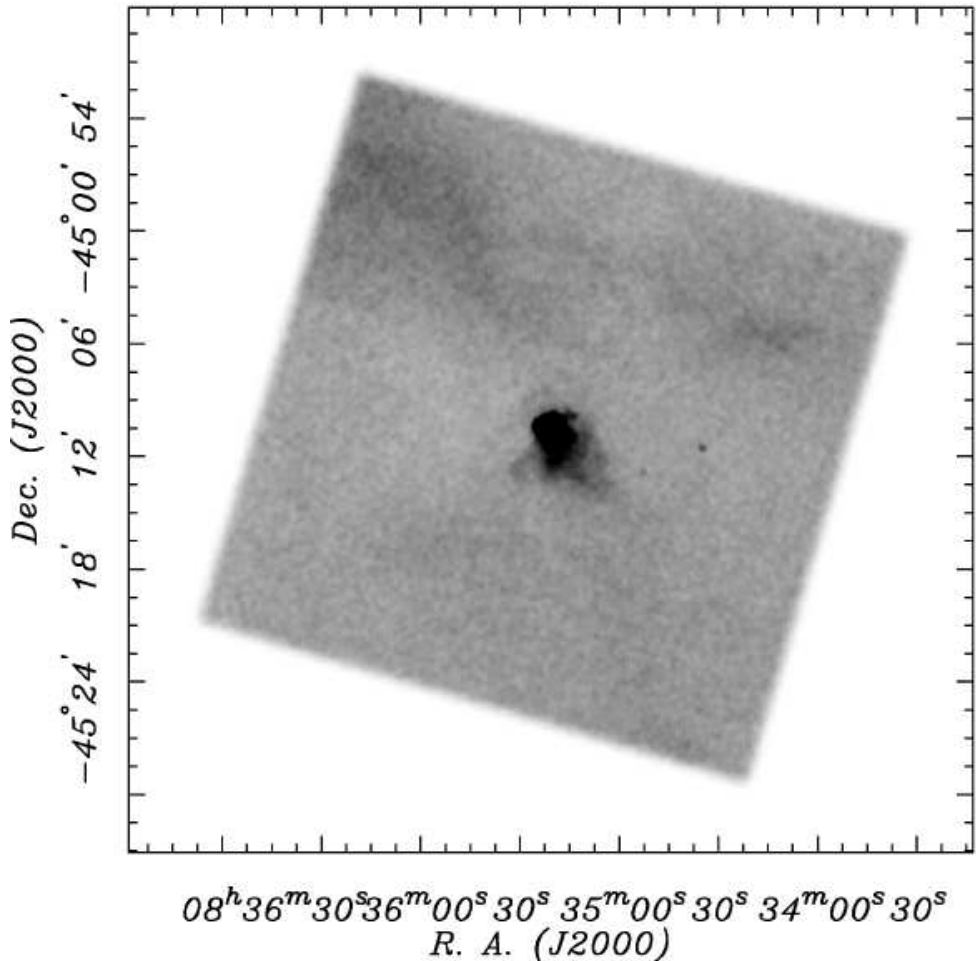


FIG. 1.— X-ray intensity distribution in the region containing the Vela pulsar PSR B0833-45. This *Chandra* High Resolution Camera (HRC) X-ray image (.1-10 keV) is smoothed and centered on the pulsar. The intensity scale is chosen to highlight the diffuse SNR emission surrounding the bright pulsar nebular, which is fully saturated in this image.

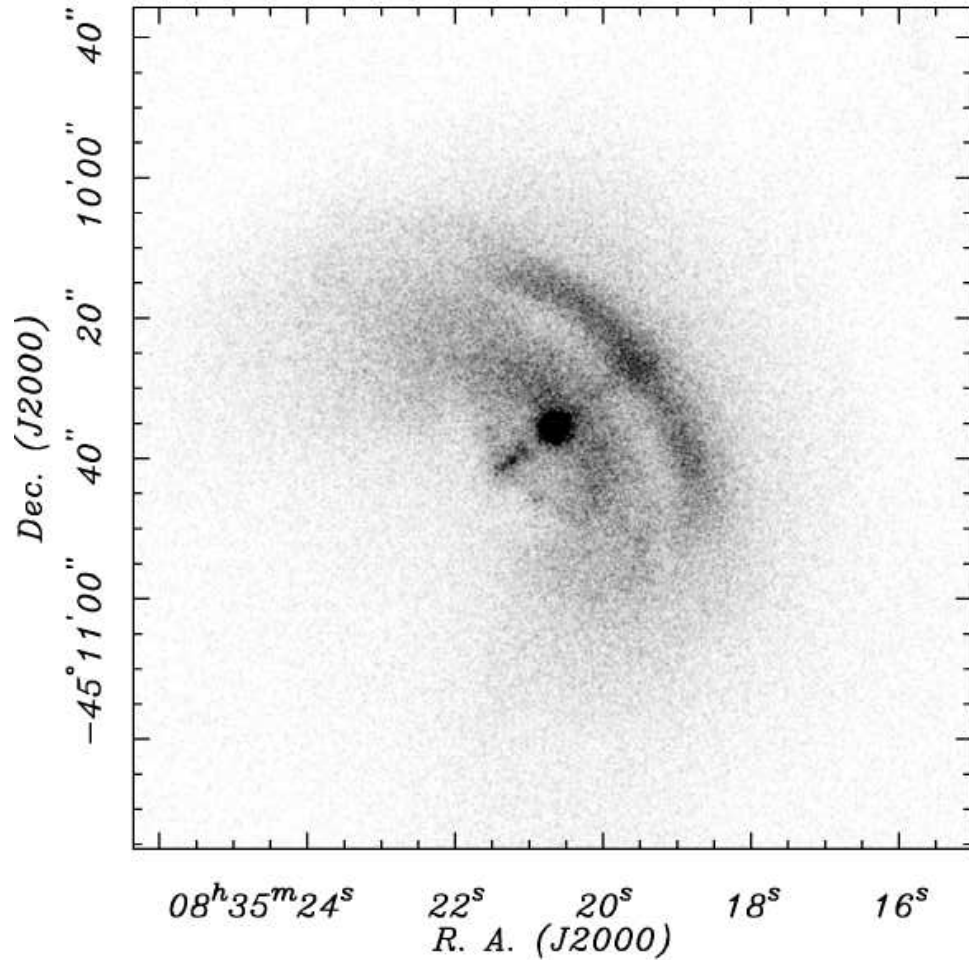


FIG. 2.— A close-up view of the region surrounding the Vela pulsar PSR B0833-45. The plot includes the summed data from two epochs separated by a month and is centered on the pulsar and scaled to highlight the surrounding nebula emission. A toroidal structure and perpendicular jet similar to that seen in the Crab Nebula is apparent. Also evident is a faint halo of emission likely associated with the post-shock pulsar wind (see text).

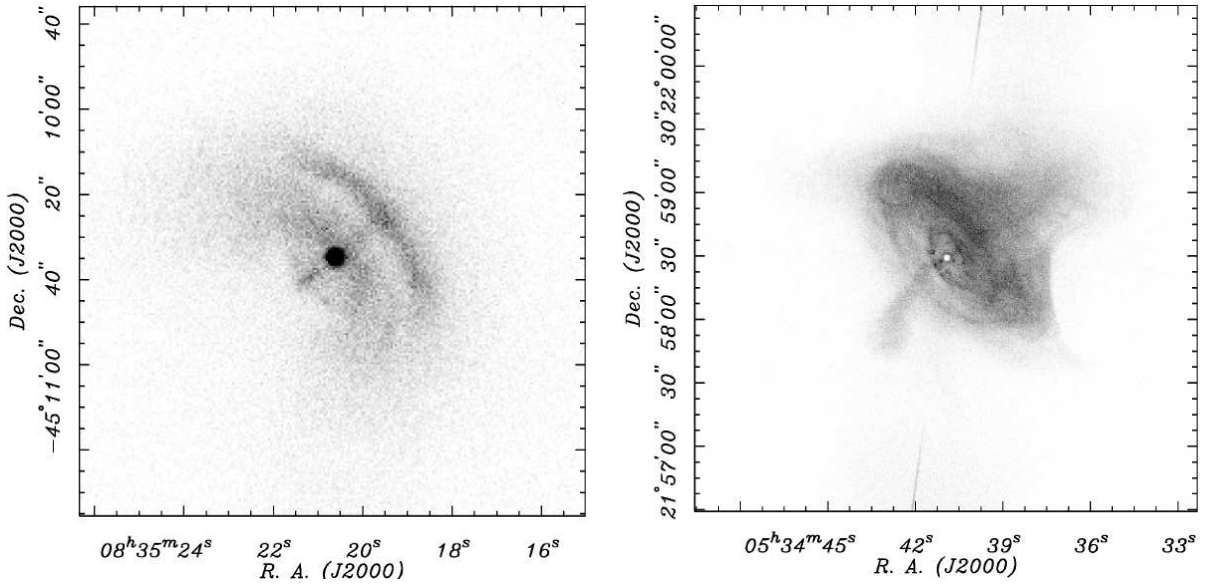


FIG. 3.— A scaled comparison of two young pulsars observed by the *Chandra* Observatory. The image of the 2 kyr old Crab nebula (left) and the 10 kyr old Vela pulsar (right) have been scaled to be the same image size. In fact, the Vela image is a factor of 16 times smaller than the Crab assuming distances of 2 kpc (Crab) and 250 pc (Vela). Although Vela is an order of magnitude older and smaller, note the similar shape and overall brightness distribution of the two objects.

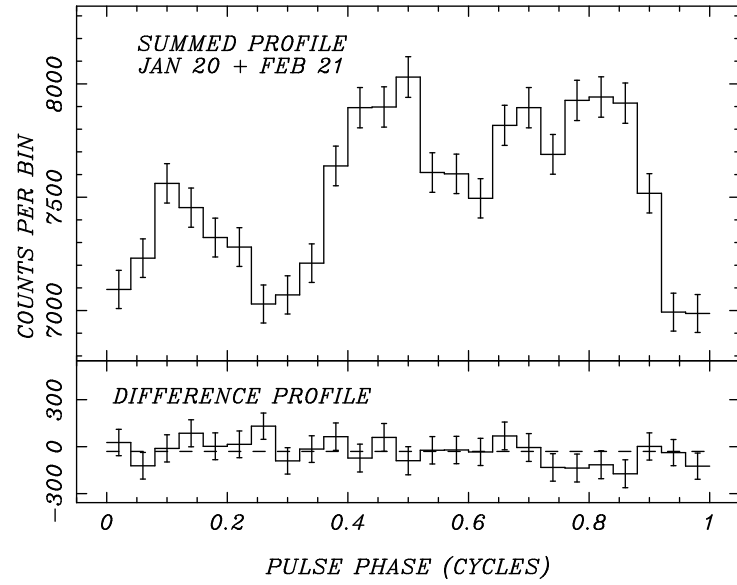


FIG. 4.— The X-ray (0.2 – 10 keV) pulse profile of the Vela pulsar obtained with the *Chandra* HRC from the combined observations (top panel) and the difference profile, observation 2 - observation 1, (bottom panel). There is no significant pulse shape change at any phase.

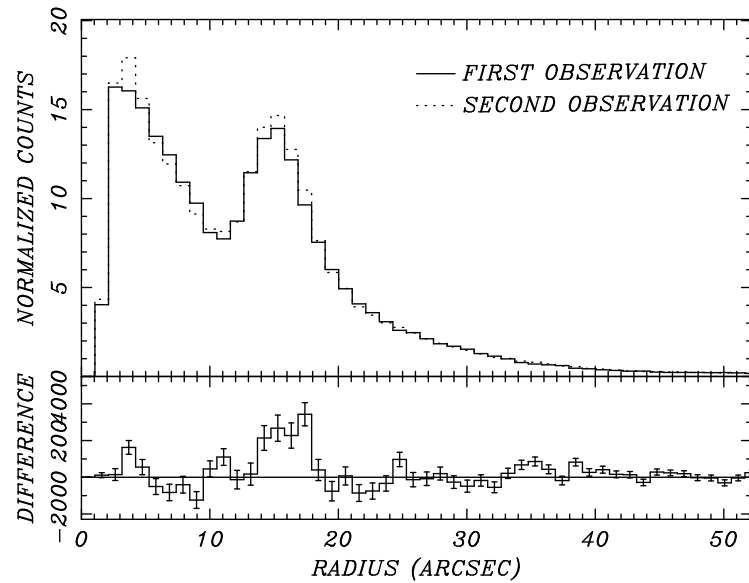


FIG. 5.— The nebular radial profile in elliptical annuli centered on the pulsar and encompassing the sector centered on the bright outer ring. Note the 7.8σ excess in observation 2 between $13\text{''}5$ and $18\text{''}0$ from the pulsar.

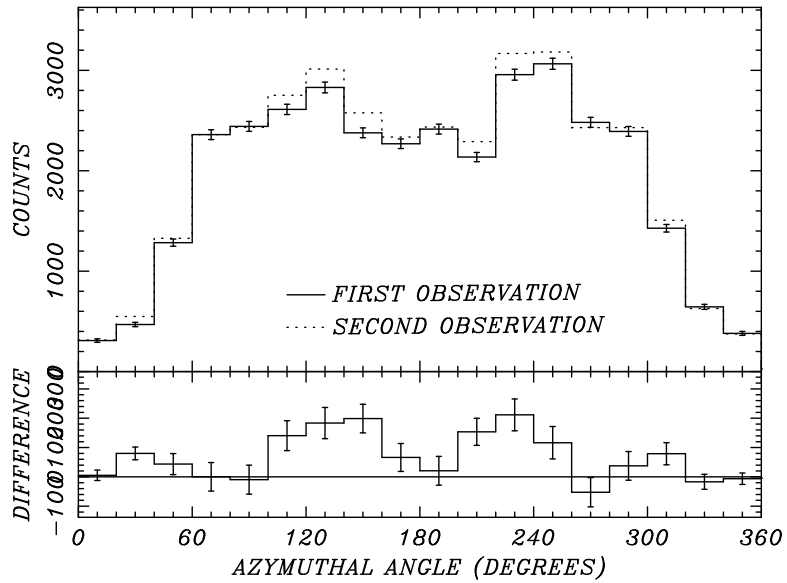


FIG. 6.— The azimuthal distribution of surface brightness in an elliptical annular ring between $13\text{''}5$ and $18\text{''}0$ from the pulsar. The ordinate gives the angle relative to the jet measured clockwise; North is at 130° here. In the range 110° to 260° , there is a 7.6σ excess in the second observation, representing a brightening of the nebula at roughly half the light travel time from the pulsar.

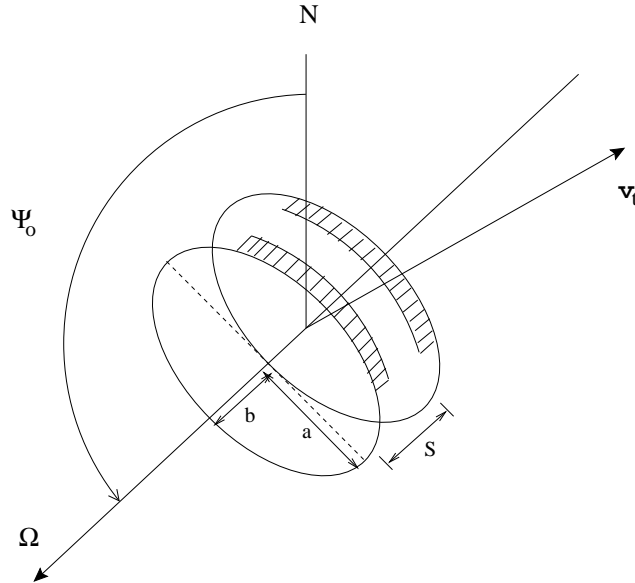


FIG. 7.— An idealized geometry for the Vela X-ray nebula as seen in the *Chandra* images. The two bright wisps are assumed to lie on the front surface of an equatorial, toroidal wind whose axis of symmetry is the rotation axis Ω of the neutron star. a and b are the semi-major and semi-minor axes of the projected ellipses, and s is the projected distance between them. For scaling, $a = 35''$ translates to 1.31×10^{17} cm at an assumed distance of 250 pc. The vector v_t is the direction of proper motion of the pulsar.

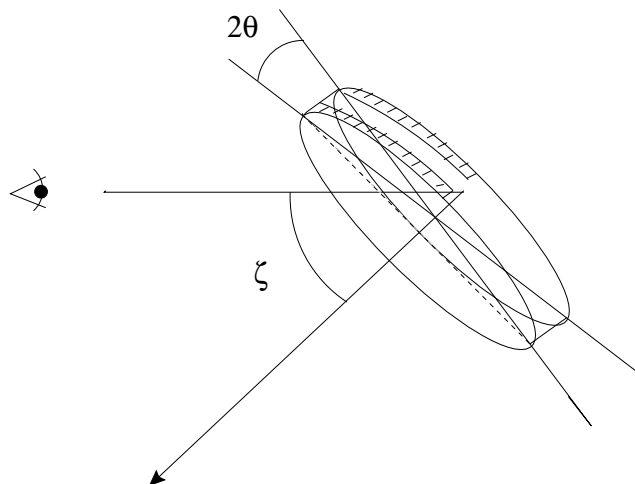


FIG. 8.— A side view of Figure 7 showing the definitions of the angles between the rotation axis Ω , the magnetic axis μ , and the line of sight. The angle ζ is inferred both from radio pulse polarization measurements, and from deprojection of the X-ray structures. The angle α is only approximately known.